Sensors and Materials, Vol. 38, No. 1 (2026) 137–147
MYU Tokyo

S & M 4290

Development of a Capacitive Humidity Sensor Based on Polyimide/Carbon Nanotube (CNT) Composite Thin Films with High CNT Content

Tatsuya Fujii,* Masaaki Takita, Tsunehisa Suzuki, and Mitsuyoshi Nomura

Department of Mechanical Engineering, Faculty of Systems Science and Technology, Akita Prefectural University, 84-4 Ebinokuchi, Tsuchiya, Yurihonjo-shi, Akita 015-0055, Japan

(Received October 15, 2025; accepted December 3, 2025)

Keywords: capacitive humidity sensor, composite thin film, polyimide, carbon nanotube, high concentration

In this study, targeting applications in flexible electronic devices, we developed and evaluated a capacitive humidity sensor with high sensitivity and excellent linearity, employing a polyimide (PI)/carbon nanotube (CNT) composite thin film containing uniformly dispersed CNTs at high concentrations. The humidity-sensitive layer was fabricated using a proprietary dispersion and film-forming method, whereas interdigitated comb-shaped electrodes were created through semiconductor microfabrication techniques. A series of sensors were fabricated with varying electrode geometries (characterized by the dimensionless parameters r and h) and CNT contents ranging from 0 to 20 wt%. The sensors were evaluated on the basis of their capacitive response to humidity, linearity, hysteresis, and response speed. The results showed that miniaturization of the electrode geometry improved sensitivity, and the optimal performance—characterized by high sensitivity, excellent linearity, and low hysteresis—was achieved at a CNT content of 10 wt%. Compared with the CNT-free sensor, the 10 wt% CNT-containing sensor exhibited a 14.4-fold increase in sensitivity and a 4.6-fold increase in the maximum capacitance change rate. These findings contribute to the development of humidity monitoring technologies suitable for integration into component-embedded flexible substrates and provide a fundamental basis for advancing flexible sensor technologies.

1. Introduction

Recently, component-embedded substrates—where electronic components such as passive and active devices, modules, and MEMS are integrated within printed circuit boards (PCBs)—have attracted significant attention as a promising packaging technology for achieving miniaturization, weight reduction, enhanced performance, and improved reliability in electronic systems. As components continue to shrink, embedding them into flexible PCBs (FPCs) has become feasible, enabling novel applications that leverage the thinness and flexibility of these substrates. This advancement is expected to drive innovations in wearable, medical, and

*Corresponding author: e-mail: t-fujii@akita-pu.ac.jp
https://doi.org/10.18494/SAM5981

ISSN 0914-4935
https://myukk.org/

healthcare devices. However, when component-embedded substrates are used in flexible devices, repeated mechanical deformation—such as bending, stretching, and twisting—can cause delamination of adhesive layers within the substrate, increasing the risk of internal component failure. Therefore, the reliability and lifespan of such flexible systems depend heavily on the robustness of the packaging technology.

In this context, humidity monitoring using sensors based on polymeric humidity-sensitive materials has been proposed as a means of assessing the health of embedded components and detecting internal abnormalities at an early stage. Although polyimide (PI) films have been used in resistive-type humidity sensors owing to their hygroscopic nature, these sensors typically exhibit an exponential change in resistance with humidity, resulting in poor accuracy—particularly at relative humidity (RH) levels below 30%. Yoo *et al.* reported that incorporating carbon nanotubes (CNTs) into PI films enhances their electrical conductivity and improves the linearity of sensor output.[1] However, owing to the strong tendency of CNTs to agglomerate, achieving homogeneous nanoscale dispersion—especially at high concentrations—remains extremely challenging, making the fabrication of high-CNT-content PI films difficult.[2] Kim *et al.* demonstrated that capacitive-type humidity sensors with parallel-plate electrodes offer better sensitivity and linearity than resistive types, but their complex fabrication processes and susceptibility to electrode damage present significant drawbacks.[3] Moreover, capacitive humidity sensors employing interdigitated comb-shaped electrodes have been examined in only a few studies, none of which have analyzed in detail the humidity response characteristics of PI/CNT composite thin films with high CNT content.[4–7] Therefore, to establish a humidity monitoring technology suitable for component-embedded flexible substrates, it is essential to quantitatively evaluate the humidity response of PI/CNT composite films and to develop a novel capacitive humidity sensor that is compatible with flexible electronics.

In this study, we aim to develop a high-performance PI-based capacitive humidity sensor enhanced through CNT integration. To this end, PI/CNT composite films with uniformly dispersed CNTs at high concentrations were fabricated using a novel film-forming technique. This approach enables a significant increase in capacitance variation, which has traditionally been difficult to achieve owing to CNT aggregation. Furthermore, by employing interdigitated electrodes, we aim to improve the linearity of the humidity response in capacitive measurements.

2. Experimental Procedure

Figure 1 shows a schematic of the capacitive humidity sensor fabricated in this study. The sensor comprises interdigitated comb electrodes formed on an insulating substrate using semiconductor processing techniques, with a PI/CNT composite thin film deposited as the humidity-sensitive layer. The dimensions of the sensing film were set to 4.8 mm (length) × 6.0 mm (width). Capacitive humidity sensors detect humidity by measuring changes in capacitance resulting from variations in the dielectric constant of the sensing film as it absorbs or releases moisture. To investigate the effects of electrode geometry and CNT content on humidity response, sensors were fabricated under various conditions. The geometry of the comb electrodes is defined by the electrode width, gap, and number of comb fingers. In capacitive measurements

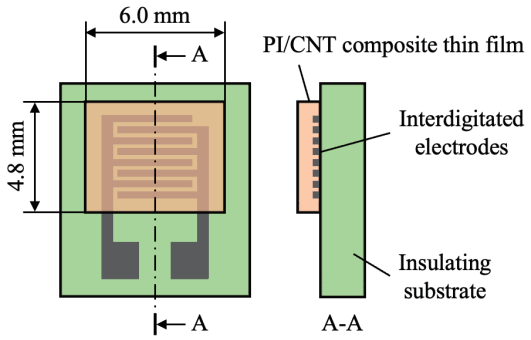

Fig. 1. (Color online) Schematic of the capacitive humidity sensor.

using interdigitated electrodes, changes in the dielectric constant of the sensing film within the electric field between the electrodes are detected. Therefore, the swelling or shrinking of the film during moisture absorption or desorption significantly affects sensor sensitivity. Previous studies have also shown that electrode geometry affects sensor performance.[8–12] To evaluate this effect, electrodes of eight different configurations were fabricated, as illustrated in Fig. 2 and summarized in Table 1. The sensing area was fixed at 3.0 mm × 4.0 mm. Two dimensionless parameters were introduced to evaluate the electrode design.

$$r = h / \{2(w + g)\} \tag{1}$$

$$h = w / (w + g) \tag{2}$$

Here, h is the thickness of the sensing film (design value: 3 mm), w is the electrode width, and g is the electrode gap. The parameter r represents the ratio of film thickness to the combined width and gap of the electrodes, with larger values indicating finer electrode structures. The parameter h denotes the ratio of electrode width to the total pitch (width plus gap). The parameter r does not have a standard name in the literature and is defined here as a convenient measure relating the film thickness to the electrode dimensions. In contrast, the parameter h is the commonly used fill factor, representing the fraction of each electrode period occupied by the electrode. These parameters were used to quantitatively assess the effect of electrode geometry on sensor performance.

Owing to the strong tendency of CNTs to agglomerate, achieving stable dispersion at high concentrations in polymer matrices remains particularly challenging. In this study, we adopted a fabrication method involving the coating of CNTs with polyamic acid (PAA), the precursor of PI, to produce PAA-coated CNT particles.[13] The preparation method for these particles is illustrated in Fig. 3(a). A solution of PAA in N-methyl-2-pyrrolidone (NMP) (UBE, U-Varnish-A) was mixed with a dispersion of multiwalled CNTs (MWCNTs) in NMP (Nanocyl, NMP0502) to obtain a CNT-to-PAA weight ratio of 30 wt%. The mixture was then ultrasonicated using a 400 W homogenizer (Hielscher, UP400S) with intermittent cooling to prevent overheating. The

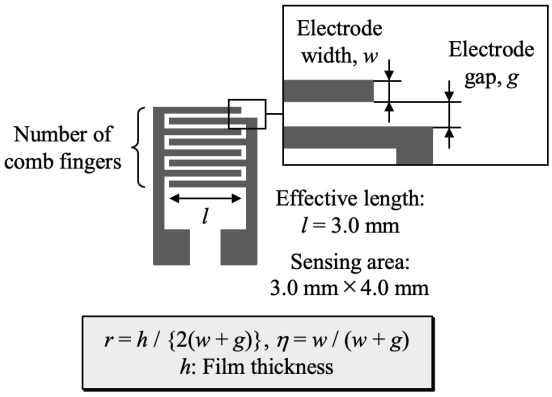

Fig. 2. Design parameters of interdigitated electrodes.

Table 1
Combination of electrode parameters.

r	Width, w (μm)	Gap, g (μm)	Number of fingers
0.06	12.5	12.5	160
0.075	10	10	200
0.1	7.5	7.5	266
0.15	5	5	400

η	Width, w (μm)	Gap, g (μm)	Number of fingers
0.3	4.5	10.5	266
0.4	6	9	266
0.5	7.5	7.5	266
0.6	9	6	266

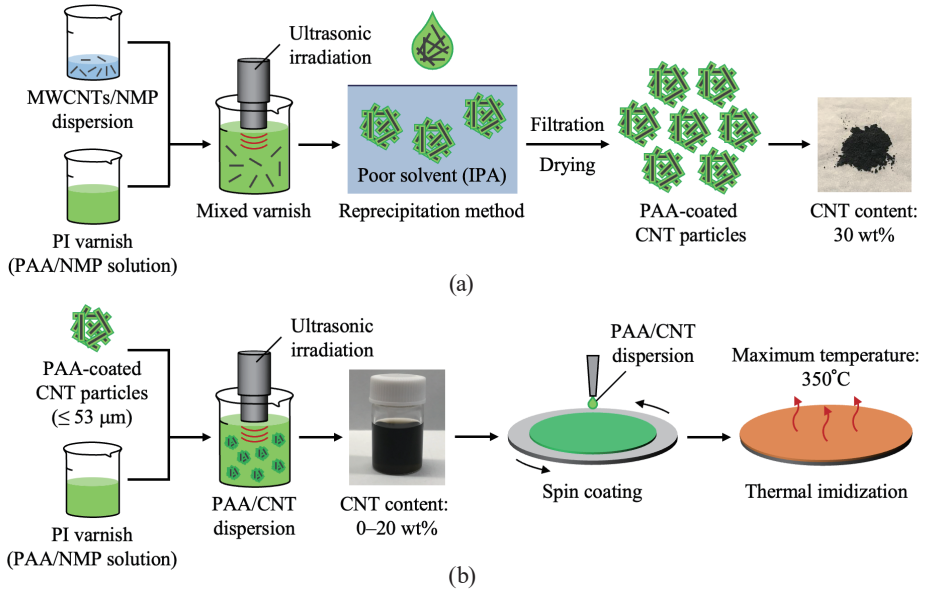

Fig. 3. (Color online) (a) Preparation method for PAA-coated CNT particles. (b) Fabrication process for PI/CNT composite thin films from the PAA/CNT dispersion.

sonication process consisted of two cycles of 30 s of sonication followed by 5 min of cooling. The MWCNTs used in this study had a diameter of 9.5 nm and a length of 1–2 mm. They were synthesized by catalytic chemical vapor deposition (Cat-CVD).[14] The resulting PAA/CNT dispersion was added dropwise into a poor solvent, isopropyl alcohol (IPA), to remove NMP. The mixture was then subjected to vacuum filtration and air drying, yielding PAA-coated CNT particles. This precipitation method does not require surfactants and relies on differences in solvent polarity to induce particle formation.

The process for fabricating PI/CNT composite thin films from the PAA/CNT dispersion is illustrated in Fig. 3(b). The dried particles were pulverized using a mortar and sieved to collect those smaller than 53 mm. These particles were then re-dispersed in a PAA/NMP solution to prepare dispersions with CNT concentrations of 0, 5, 10, and 20 wt%, using a 200 W ultrasonic homogenizer (Hielscher, UP200St) for a total treatment time of 24 min. The total solid content and dispersion volume were adjusted by varying the amount of NMP. The films were formed by spin coating, which enables uniform film thickness through radial spreading induced by centrifugal force. After coating, thermal imidization was carried out to convert PAA into PI. This reaction proceeds via nucleophilic attack of the amide nitrogen on the carboxylic acid group, followed by dehydration and ring closure. Since the properties of PI are highly dependent on the imidization temperature,[15,16] the films were gradually heated from 80 to 350 °C on a hotplate to prevent defects and bubble formation caused by rapid solvent evaporation.

The fabrication process for the PI/CNT capacitive humidity sensor is illustrated in Fig. 4(a). The sensor was fabricated using semiconductor microfabrication techniques on a silicon wafer with a 350-nm-thick thermally grown SiO_2 insulating layer. First, a negative photoresist (Zeon, ZPN1150-90) was patterned by photolithography to define the electrode geometry. Next, a 10-nm-thick titanium (Ti) adhesion layer and a 100-nm-thick gold (Au) layer were sequentially deposited using a sputtering system (Canon Anelva, E-200S). The Ti layer was introduced to improve adhesion between the Au layer and the silicon wafer. Following deposition, a lift-off process was used to remove the unwanted photoresist and the metal layers above it, resulting in

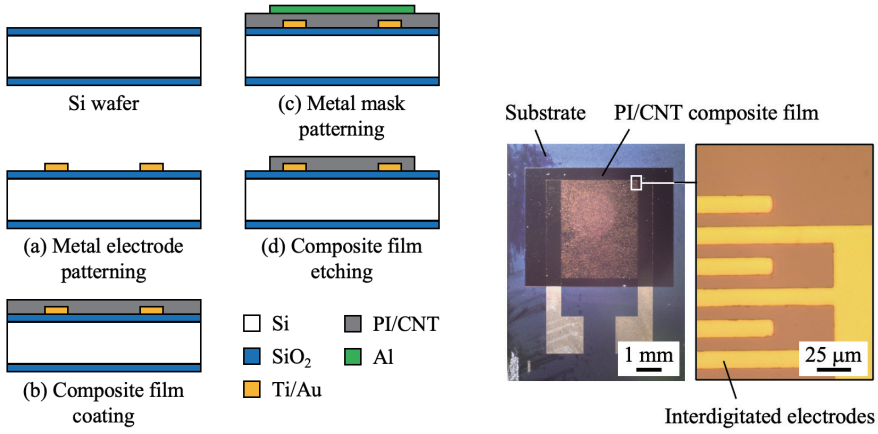

Fig. 4. (Color online) (a) Fabrication process for the PI/CNT capacitive humidity sensor using semiconductor microfabrication techniques. (b) Photograph of the fabricated PI/CNT capacitive humidity sensor.

the formation of interdigitated electrodes. Subsequently, the PI/CNT composite film was formed from the PAA/CNT dispersions prepared as described in the previous section. To enhance adhesion between the substrate and the composite film, a silane coupling agent (Shin-Etsu Chemical, KBE-903), diluted to 1% with ethanol, was applied to the substrate using a spin coater. Insufficient contact between the sensing film and the electrodes can reduce the effective electrode area and prevent changes in the film's dielectric constant from being accurately reflected in the sensor response. Four types of PAA/CNT dispersion preparation with CNT concentrations of 0, 5, 10, and 20 wt% were then spin-coated onto the treated substrate. After coating, thermal imidization was performed on a hotplate to convert the PAA/CNT films into PI/CNT composite films. Optical microscopy and SEM observations of the film surface revealed no noticeable delamination, indicating that the adhesion between the sensing film and the electrodes is sufficient to maintain stable sensor performance. A 100-nm-thick aluminum (Al) layer was then deposited by sputtering and patterned by photolithography to serve as an etching mask for patterning the composite film. The exposed areas of the PI/CNT composite film were removed using O_2 plasma in a plasma dry cleaner (Yamato Scientific, PDC210). Finally, the Al mask was removed, completing the sensor fabrication process. A photograph of the fabricated PI/CNT capacitive humidity sensor is shown in Fig. 4(b).

The humidity response of the fabricated sensors was evaluated by measuring capacitance changes under various humidity conditions using a custom-built humidity control system (control range: 10–85% RH) and an LCR meter (NF, ZM2376). A schematic of the measurement setup is shown in Fig. 5. Humidity was controlled by mixing two airflows: dry air passed through silica gel (Fujigel Sangyo, PQ3–5mmB) and humid air generated by bubbling air through water. The flow rates of the two airflows were adjusted using flow meters (Kofloc, RK1710), then mixed in a chamber to supply air at the desired RH. The fabricated sensors were diced into chips and mounted onto a universal breadboard (Sunhayato, SAD-101) using one-touch connectors (Sunhayato, SAK-1-1). Conductive paste (Fujikura Kasei, D-550) was applied to the electrode pads to ensure reliable electrical contact. The humidity response was evaluated by monitoring capacitance changes using the LCR meter. To monitor ambient humidity and verify its correlation with the sensor output, a commercial humidity sensor (Sato Keiryoki Mfg, SK-L754) was placed in proximity to the test device. Measurements were conducted in an

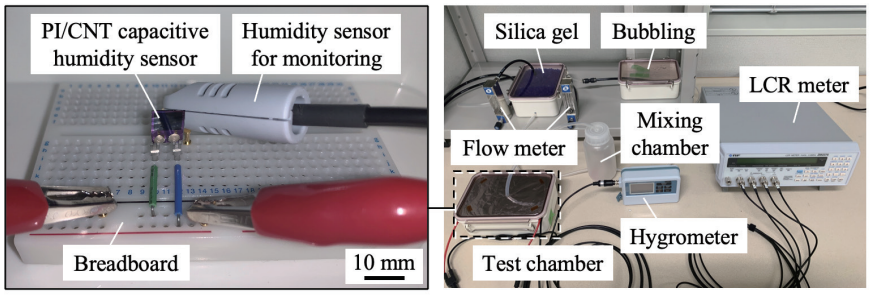

Fig. 5. (Color online) Schematic of the measurement setup for evaluating humidity response using a custom-built humidity control system (control range: 10–85% RH) and an LCR meter.

environment maintained at 25 ℃, with RH continuously varied from 10 to 85% RH. The LCR meter was operated at a frequency of 1 kHz with an applied voltage of 1 V.

3. Results and Discussion

Figures 6(a) and 6(b) show the humidity dependence of capacitance variation for sensors with sensing films and 5 wt% CNT content and different electrode design parameters. In both figures, the vertical axis represents the change in capacitance relative to the baseline at 10% RH, whereas the horizontal axis indicates the RH. The legends indicate the capacitance variation ratio, calculated from the capacitance values at 10% RH and 85% RH. From Fig. 6(a), it can be observed that increasing the parameter r (i.e., miniaturizing the electrode structure) leads to an increase in both the absolute capacitance variation and variation ratio. This is attributed to the enhanced electric field concentration between the electrodes, enabling the more sensitive detection of changes in the dielectric constant of the sensing film. Figure 6(b) illustrates the relationship between humidity response and the parameter h (the ratio of electrode width to the total pitch) of the interdigitated electrodes. An h value of 0.5 corresponds to a 1:1 width-to-gap ratio. The results indicate that h does not significantly affect the magnitude of capacitance change or the linearity with respect to humidity. However, a decreasing trend in the capacitance variation ratio was observed as h decreased. This is likely due to a reduction in the baseline capacitance, meaning that for a similar absolute capacitance change, the relative variation becomes larger. On the basis of these results and fabrication yield considerations, sensors fabricated with r = 0.075 and h = 0.3 were selected for evaluating the effect of CNT content on sensor performance.

Figures 7(a) and 7(b) show the humidity dependence of capacitance for sensors with sensing films and various CNT concentrations. An increase in CNT content led to a corresponding increase in both the capacitance change and the variation ratio. However, for the sensor with 20 wt% CNT content, although the capacitance variation increased, the humidity response exhibited noticeable nonlinearity. This nonlinearity may be attributed to measurement

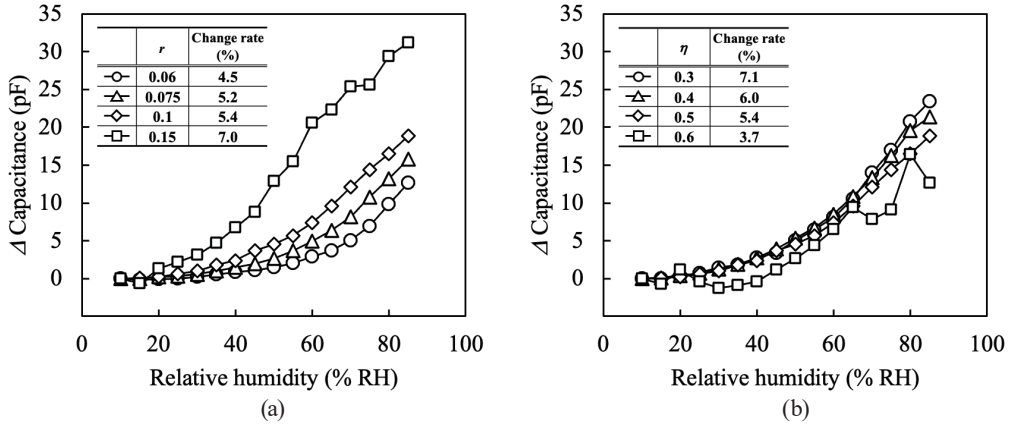

Fig. 6. Humidity dependence of capacitance variation for sensors with sensing films and 5 wt% CNT content, shown for different electrode design parameters: (a) r and (b) η.

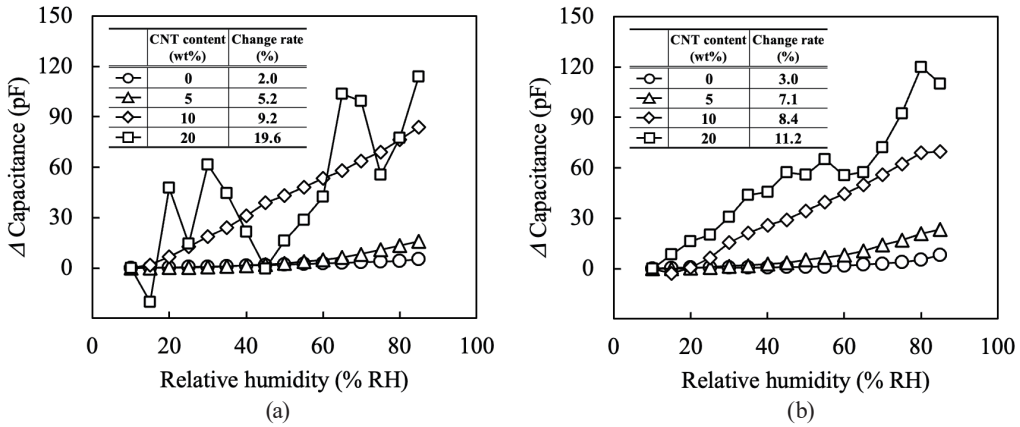

Fig. 7. Humidity dependence of capacitance for sensors employing sensing films with various CNT concentrations, shown for each electrode parameter: (a) $r = 0.075$ and (b) $\eta = 0.3$.

instability, possibly caused by fluctuations in the electrical resistance of the sensing film. The measured resistances of the films at 15% RH were approximately 18 MW (0 wt%), 13 MW (5 wt%), 9.4 kW (10 wt%), and 40 W (20 wt%). As the CNT concentration increases, the inter-CNT distance decreases, promoting the formation of a conductive network. Consequently, small variations in inter-CNT distance—caused by the expansion and contraction of the PI matrix or the formation of conductive paths via absorbed moisture—can lead to measurement instability. From these observations, a CNT content of 10 wt% was identified as optimal, and comparative evaluations were conducted against a 0 wt% CNT (pure PI) sensor. Compared with the 0 wt% CNT-containing sensor, the capacitance variation ratio increased by approximately 4.6 times for $r = 0.075$ and by about 2.8 times for $h = 0.3$. Sensors with intermediate CNT contents, such as 15 wt%, were not investigated in this study. However, based on the results for the 10 and 20 wt% sensors, the transition from linear to nonlinear humidity response is expected to occur within this intermediate CNT concentration range.

Figures 8(a) and 8(b) show the hysteresis characteristics of PI/CNT humidity sensors with 0 and 10 wt% CNT contents. The vertical axis represents capacitance, whereas the horizontal axis indicates RH; the data points differentiate between the absorption and desorption processes. Significant hysteresis was observed in the 0 wt% CNT-containing sensor, particularly at both low- and high-RH ranges. In contrast, the 10 wt% CNT-containing sensor exhibited reduced hysteresis, mainly during the desorption process at a low RH. Both sensors displayed good linearity across the tested RH range, demonstrating the effectiveness of the interdigitated electrode structure in maintaining capacitive linearity. Notably, the 10 wt% CNT-containing sensor exhibited improved linearity compared with the pure PI sensor. The sensitivity, defined as the capacitance change per % RH, was 0.078 pF/% RH for the 0 wt% CNT-containing sensor and 1.126 pF/% RH for the 10 wt% CNT-containing sensor, indicating an approximately 14.4-fold increase in sensitivity attributable to the addition of CNTs.

Figures 9(a) and 9(b) show the response times during the absorption and desorption processes for sensors with 0 and 10 wt% CNT contents. The vertical axis represents normalized

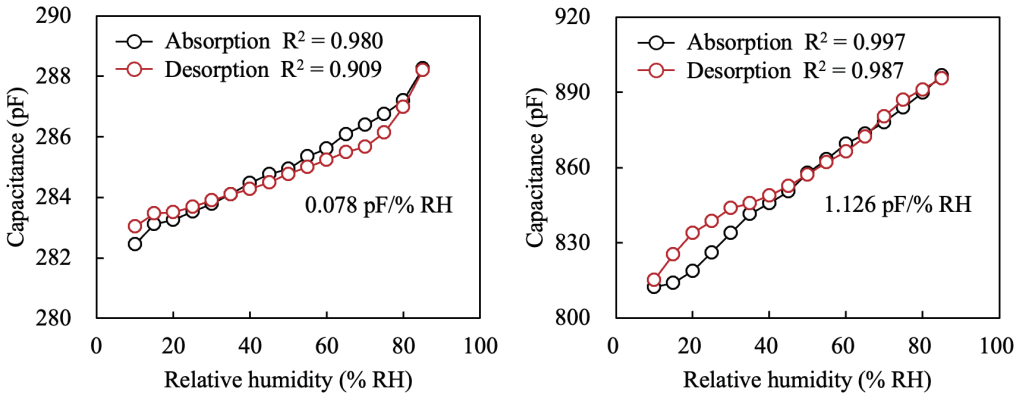

(a) (b)

Fig. 8. (Color online) Hysteresis characteristics of PI/CNT humidity sensors with CNT contents of (a) 0 and (b) 10 wt%.

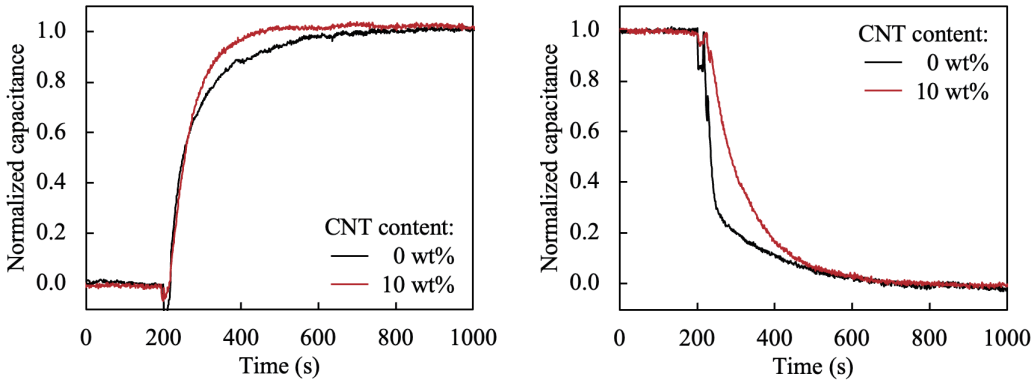

(a) (b)

Fig. 9. (Color online) Response times during (a) absorption and (b) desorption processes for sensors with 0 and 10 wt% CNT contents.

capacitance, whereas the horizontal axis indicates time. An RH change from 17.4 to 82.6% was confirmed using a commercial humidity sensor. The transition between absorption and desorption occurred 200 s after the start of the measurement. For the 0 wt% CNT-containing sensor, the response was faster during desorption than during absorption. In contrast, the 10 wt% CNT-containing sensor exhibited a faster response during absorption. Specifically, the response time to reach 63.2% of the total capacitance change improved from 80 to 76 s during absorption but increased from 30 to 97 s during desorption. These results indicate that the addition of CNTs slightly accelerated the absorption response but tended to slow down the desorption response. Compared with typical PI-based humidity sensors,[17–22] which exhibit response times of approximately 10–80 s, the PI/CNT composite sensors developed in this study showed slightly longer response times. This is likely due to the low water absorption rate of the UBE PI used, which is 1.4% at a thickness of 25 mm—lower than that of DuPont's Kapton (2.3% at 25 mm)—resulting in delayed moisture absorption and desorption behavior.[23] Although the

desorption response time increased with CNT addition, this does not significantly affect the performance of the PI/CNT capacitive humidity sensor, for which rapid response to increasing humidity is the primary requirement. The observed desorption time remains within a practically acceptable range, and the high-concentration CNT dispersion enhances the capacitance change and improves the absorption response. Therefore, the slower desorption response does not impose a critical limitation on the main objectives of this study.

4. Conclusions

In this study, we developed a capacitive humidity sensor based on a PI/CNT composite film with interdigitated electrode structures. By optimizing the film fabrication process, we achieved high-content CNT loading (up to 20 wt%) with uniform dispersion, enabling a comprehensive evaluation of the composite films' sensing performance. Among all the tested conditions, the sensor with 10 wt% CNT content exhibited the best performance, demonstrating excellent linearity and significantly enhanced sensitivity. Compared with the CNT-free sensor, the 10 wt% CNT-containing sensor showed up to a 4.6-fold increase in capacitance variation ratio and an approximately 14.4-fold improvement in sensitivity. Hysteresis and response time measurements further confirmed the positive impact of CNT incorporation, with the 10 wt% CNT-containing sensor exhibiting reduced hysteresis and a slightly faster response during absorption. However, the desorption response was slower, indicating some limitations inherent to the material properties. Overall, these findings provide valuable insights into the design of high-performance capacitive humidity sensors, particularly for integration into embedded components and flexible substrates. Future work will focus on improving response speed and enhancing environmental durability to enable practical applications.

Acknowledgments

This work was supported by the Japan Society for the Promotion of Science (JSPS) Grants-in-Aid for Scientific Research (JSPS KAKENHI Grant Number JP20K14628).

References

1 K.-P. Yoo, L.-T. Lim, N.-K. Min, M. J. Lee, C. J. Lee, and C.-W. Park: Sens. Actuators, B **145** (2010) 120. https://doi.org/10.1016/j.snb.2009.11.041
2 Q.-Y. Tang, Y. C. Chan, and K. Zhang: Sens. Actuators, B **152** (2011) 99. https://doi.org/10.1016/j.snb.2010.09.016
3 J.-H. Kim, S.-M. Hong, B.-M. Moon, and K. Kim: Microsyt. Technol. **16** (2010) 2017. https://doi.org/10.1007/s00542-010-1139-0
4 B. Adhikari and S. Majumdar: Prog. Polym. Sci. **29** (2004) 699. https://doi.org/10.1016/j.progpolymsci.2004.03.002
5 H. Bai and G. Shi: Sensors **7** (2007) 267. https://doi.org/10.3390/s7030267
6 R. H. Bhuiyan, R. A. Dougal, and M. Ali: IEEE Sens. J. **7** (2007) 1589. https://doi.org/10.1109/JSEN.2007.908440
7 N. Afsarimanesh, A. Nag, M. E. E. Alahi, T. Han, and S. C. Mukhopadhyay: Sens. Actuators, A **305** (2020) 111923. https://doi.org/10.1016/j.sna.2020.111923
8 R. Igreja and C. J. Dias: Sens. Actuators, A **112** (2004) 291. https://doi.org/10.1016/j.sna.2004.01.040
9 F. Molina-Lopez, D. Briand, and N. F. de Rooij: Sens. Actuators, B **166**–**167** (2012) 212. https://doi.org/10.1016/j.snb.2012.02.042

10 A. Rivadeneyra, J. Fernandez-Salmeron, M. Agudo-Acemel, J. A. Lopez-Villanueva, L. F. Capitan-Vallvey, and A. J. Palma: Sens. Actuators, A **244** (2016) 56. https://doi.org/10.1016/j.sna.2016.03.023
11 S. Deshpande, S. Bhand, and G. Bacher: J. Appl. Electrochem. **51** (2021) 893. https://doi.org/10.1007/s10800-021-01549-x
12 T. M. Reader, U. Hanke, E. Halvorsen, and T. Grande: Smart Mater. Struct. **29** (2020) 115039. https://doi.org/10.1088/1361-665X/abb4b9
13 T. Izunome, T. Suzuki, and Y. Otsuka: Japan Patent JP2019178027A, Published 2019-10-17.
14 H. Matsumura: Jpn. J. Appl. Phys. **37** (1998) 3175. https://doi.org/10.1143/JJAP.37.3175
15 M. Kotera, T. Nishino, and K. Nakamae: Polymer **41** (2000) 3615. https://doi.org/10.1016/S0032-3861(99)00546-7
16 X. Chen, J. Yang, and J. Zhao: Polymer **143** (2018) 46. https://doi.org/10.1016/j.polymer.2018.04.005
17 J. Kim, J.-H. Cho, H.-M. Lee, and S.-M. Hong: Sensors **21** (2021) 1974. https://doi.org/10.3390/s21061974
18 M. Dokmeci and K. Najafi: J. Microelectromech. Syst. **10** (2001) 197. https://doi.org/10.1109/84.925735
19 K. S. Choi, D. S. Kim, H. J. Yang, M. S. Ryu, and S. P. Chang: RSC Adv. **61** (2014) 32075. https://doi.org/10.1039/C4RA02692F
20 J. Boudaden, M. Steinmabl, H.-E. Endres, A. Drost, I. Eisele, C. Kutter, and P. Muller-Buschbaum: Sensors **18** (2018) 1516. https://doi.org/10.3390/s18051516
21 L. Gu, Q.-A. Huang, and M. Qin: Sens. Actuators, B **99** (2004) 491. https://doi.org/10.1016/j.snb.2003.12.060
22 J.-H. Kim, B.-M. Moon, and S.-M. Hong: Microsyst. Technol. **18** (2012) 31. https://doi.org/10.1007/s00542-011-1373-0
23 H. Pranjoto and D. D. Denton: J. Appl. Polym. Sci. **42** (1991) 75. https://doi.org/10.1002/app.1991.070420109